ISIJ International, Vol. 57 (2017), No. 10, pp. 1774–1779

A Molecular Dynamics Study of Partitionless Solidification and Melting of Al–Cu Alloys

Sankar Kumar DEB NATH,[1)] Yasushi SHIBUTA,[2)]* Munekazu OHNO,[3)] Tomohiro TAKAKI[4)] and Tetsuo MOHRI[1)]

1) Institute for Materials Research, Tohoku University, 2-1-1 Katahira, Aoba-ku, Sendai, 980-8577 Japan.
2) Department of Materials Engineering, The University of Tokyo, 7-3-1 Hongo, Bunkyo-ku, Tokyo, 113-8656 Japan.
3) Division of Materials Science and Engineering, Faculty of Engineering, Hokkaido University, Kita 13 Nishi 8, Kita-ku, Sapporo, Hokkaido, 060-8628 Japan.
4) Faculty of Mechanical Engineering, Kyoto Institute of Technology, Matsugasaki, Sakyo-ku, Kyoto, 606-8585 Japan.

(*Received on April 20, 2017; accepted on June 13, 2017; J-STAGE Advance published date: August 24, 2017*)

The partitionless solidification and melting in Al–Cu alloy system are investigated by means of molecular dynamics simulations with an embedded atom method (EAM) potential. The solid-liquid interfacial velocity for solid-liquid biphasic systems of Al-rich alloys is examined with respect to temperature and Cu composition. The kinetic coefficient is then derived from the slope of the interfacial velocity with respect to temperature. Our results show that the kinetic coefficient is largely dependent on the Cu composition. It sharply decreases with addition of small amount of Cu. There is almost no partition at the solid-liquid interface within the time scale of the simulation since the solid-liquid interfacial velocity is very fast at temperatures away from the equilibrium temperature. Since it is not straightforward to measure the kinetic coefficient directly from experiments, it is significant in this study to derive the composition dependence of the kinetic coefficient for binary alloys directly from the MD simulation without any phenomenological parameters.

KEY WORDS: molecular dynamics simulation; Al–Cu alloys; kinetic coefficient; solid-liquid interfacial velocity.

1. Introduction

During solidification of metals and alloys, dendritic structures are formed due to the anisotropy in the solid-liquid interfacial energy and the kinetic coefficient. Although there are several experimental techniques to examine the solid-liquid interfacial properties,[1–7)] few experimental attempts were reported for the measurement of the kinetic coefficient of the solid-liquid interface.[2,3)] Due to lying solid-liquid interface between the two condensed phases, the measurement of the kinetic coefficients of the solid-liquid interface of metal and alloys using the experiment are difficult.[8)] Moreover, growth morphologies of metals[9,10)] including the dendritic growth depends on the magnitude and orientation anisotropy of their kinetic coefficients.[1)] Crystal growth morphologies in binary alloys are more complex than pure metals.[11–13)] Therefore, the solid-liquid interfacial properties have been widely studied by computational approaches.[14)]

Especially, molecular dynamics (MD) simulations have been utilized to evaluate solid-liquid interfacial properties at high temperature[15–17)] as well as to analyze the atomistic nature of solidification processes.[17–21)] MD simulations have successfully been applied to the evaluation of solid-liquid interfacial energy including the anisotropy in several metals, *e.g.*, Ni,[22–25)] Cu,[23,24)] Au,[26)] Ag,[24,26)] Al,[23,24)] Pb[23,24,27)] and Fe[28–30)] as well as the model system such as hard-sphere[31)] and Lennard-Jones systems.[32)] Importantly, the kinetic coefficients were studied for several physical systems characterized by different interatomic potentials such as Lennard-Jones potential,[33,34)] embedded atom method (EAM),[26,28,35)] Finnis-Sinclair (FS) potential[30)] and hard-sphere model.[36)] In particular, the kinetic coefficients of the solid-liquid interface in realistic materials such as Ag,[26)] Au,[26)] Cu and Ni,[35)] Ni[37)] and Fe,[28)] were estimated by using the EAM potentials. In the above studies, the thermostat set point temperatures were mainly used to obtain the kinetic coefficient from the slope of the interface velocity versus temperature relationship. On the other hand, some recent studies were carried out considering the interface temperature instead of thermostat set point temperature for determining the kinetic coefficients of several metals, *e.g.*, Ni,[38,39)] Al,[39)] Cu,[39)] Mg,[40)] Fe.[40)] The obtained kinetic coefficient using the interface temperature is around two times larger than that using the thermostat set point temperature for the case of Ni[38)] using the FBD[41)] potential. Another drawback in most of previous studies is the use of the NVT (constant number of atoms, constant volume and constant temperature) ensemble instead of the NPT (constant number of atoms, constant volume and constant pressure) ensemble,

* Corresponding author: E-mail: shibuta@material.t.u-tokyo.ac.jp
DOI: http://dx.doi.org/10.2355/isijinternational.ISIJINT-2017-221

which ensures the simulation more realistic. Besides, some of the previous studies claim that the kinetic coefficient is dependent on sizes at very small sample sizes.[42] In addition, most of these studies are limited to the estimation of the interfacial properties for pure metals except for several cases (*e.g.* $Cu_{50}Ni_{50}$[43]), whereas most of actual products consist of alloys. One of the difficulties to study the alloy system by the MD simulation is due to the deficiency of the reliable interatomic potentials. Especially, interatomic potentials for ferrous alloys and steels are not established since it is not straightforward to reproduce the effect of additive elements on thermal and mechanical properties properly. Moreover, it is still challenging to reproduce the phase transformation in iron and steel in appropriate ranges of temperature and solute composition despite of many efforts.[44–48] On the other hand, recent EAM type potentials are well tuned for many of nickel-base and aluminum-base alloy systems.[49] These benefits inspired the idea to investigate the composition dependence of the kinetic coefficient of practical alloy systematically. To these ends, the kinetic coefficient in Al rich part of Al–Cu alloys, which is one of the practical alloys, is investigated by the MD simulations in this study.

2. Simulation Methodology

The EAM potential is one of the most widely used interatomic potentials for describing the metals and alloys.[50] The total energy of an atom i is given by

$$E_i = F_\alpha\left(\sum_{j\neq i}\rho_\beta(r_{ij})\right)+\frac{1}{2}\sum_{j\neq i}\phi_{\alpha\beta}(r_{ij}) \quad \text{..... (1)}$$

where F is the embedding energy, which is a function of the electron density ρ, ϕ is a pair potential interaction, and α and β are element types of atoms i and j. The multi-body nature of the EAM potential is a result of the embedding energy term. Both summations in the formula are over all neighbors j of atom i within the cutoff distance. We employed the interatomic potentials for pure Cu and Al developed by Mendelev *et al.*[51] and Al–Cu alloys developed by Liu *et al.*[52] The LAMMPS molecular dynamics simulator[53] is used for the MD simulation. The velocity-Verlet method is used to integrate the classical equation of motion with a time step of 5.0 fs. The Nose-Hoover thermostat and barostat are employed to control temperature and pressure. The computational system consists of a rectangular box of 606.79 × 121.4 × 80.91 Å^3 ([100] along to the longest side) and 545.86 × 109.17 × 72.78 Å^3 (([110] along to the longest side)) for the case of Al system. To evaluate the composition dependence of the kinetic coefficient, the Cu composition varied from 0 to 30 at% and a pure Cu system is also employed. For alloy cases, four replicate initial configurations, which is prepared as the random mixture, are employed to consider the variety of configuration for each composition. Lattice parameters of Al–Cu alloys are calculated considering the fraction of Al and Cu in the alloys using the lattice constant of Al and Cu. The periodic boundary conditions were applied to all directions.

Initially, half atoms in the system in the middle region of the slab are heated up from 300 K to 2 000 K at the constant rate using NVT constant ensemble within 200 000 steps. During melting of the middle regions of the slabs, the rest half atoms are maintained at a constant temperature 300 K using NVT constant ensemble to create solid-liquid coexisting systems with (100) and (110) plane appearing on the interface for pure Al and Cu systems. Only systems with the (100) phase are prepared for the alloy systems. Prepared initial configurations are then heated isothermally up to a prescribed temperatures using NPT constant ensemble to observe the migration of solid-liquid interfaces. The interface velocity is estimated from the slope of the position of solid-liquid interface as a function of time, which is taken from the snapshots of each 5 000 step. The temperature dependence of the velocity is examined by repeating the same procedures at the different temperatures to derive the kinetic coefficient. The obtained atomic configuration is visualized using OVITO (Open visualization tool).[54] The adaptive common neighbor analysis (a-CNA),[55] which employs variable cutoff distances, is then performed to identify solid (*i.e.* face-centered cubic (fcc) in a-CNA) and liquid (*i.e.* unknown in a-CNA) configuration for all atoms in the calculation system. We note that determination of fcc configuration at high temperature includes the inherent error due to the thermal vibration for the CNA technique.[56]

3. Results and Discussion

3.1. Kinetic Coefficient of Pure Al and Cu

Figure 1 shows the snapshots of the movement of the solid-liquid interface with the (100) orientation in pure Al at 930 K and 960 K. At 930 K, the solid region increases with time and hence the solidification takes place. On the other hand, the liquid region increases with time by migration of the solid-liquid interface toward solid region at 960 K and hence the melting occurs at this temperature. **Figure 2** shows the time dependence of position of the solid-liquid interface at 910 K where the position monotonically increases with time. The interfacial velocity at 910 K is estimated to be approximately 15.6 m/s from the slope of the data in Fig. 2. In the same manner, the interfacial velocity was estimated for various temperatures. **Figure 3** shows the temperature dependence of the solid-liquid interfacial velocity for pure Al system for the solid-liquid interface with (100) and (110) orientations. Note that positive and negative velocities indicate melting and solidification, respectively. In the figure, the solid-liquid interfacial velocities are linearly fitted. From the slope of the linearly fitted solid-liquid interface velocity, the kinetic coefficient of the solid-liquid interface of Al for (100) and (110) orientations are estimated to be 0.433 and 0.283 m/sK, respectively. The kinetic coefficient of the solid-liquid interface of Al with the (100) orientation is higher than that of the (110) orientation, which signifies that the crystal growth of Al during solidification is dependent on crystal orientation. It basically agrees with previous reports for other pure metals.[21,23] The linearly fitted lines for (100) and (110) orientations intersect with dotted line showing the solid-liquid interface velocity to be zero at 945 K. It is defined as the melting point of pure Al for this potential, which is close to the experimental value 933.47 K. **Figure 4** illustrates the temperature dependence of the interfacial velocity for (100) and (110) orientations, respectively for pure Cu system in the same manner as pure

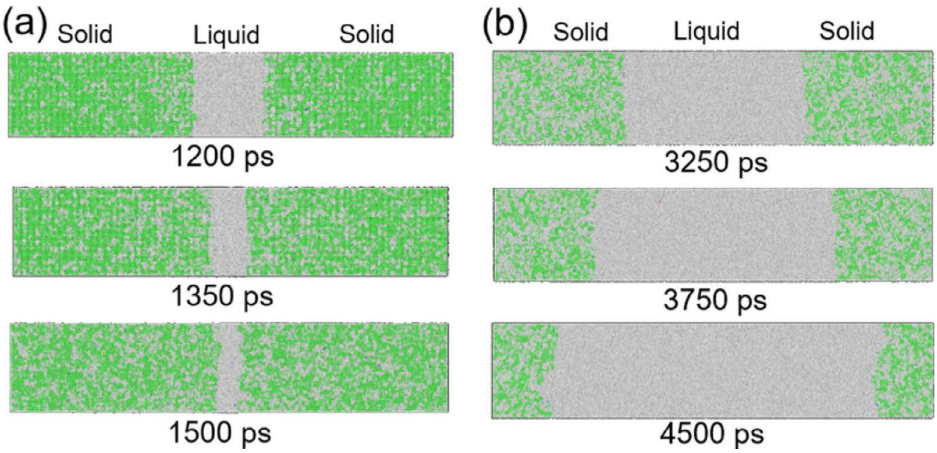

Fig. 1. Snapshots of solid-liquid biphasic system of pure Al with the (100) plane appearing on the solid-liquid interfaces at (a) 930 K and (b) 960 K, respectively. Green and white atoms represent atoms with fcc and unknown (*i.e.*, liquid) configurations defined as adaptive common neighbor analysis (a-CNA).[55] (Online version in color.)

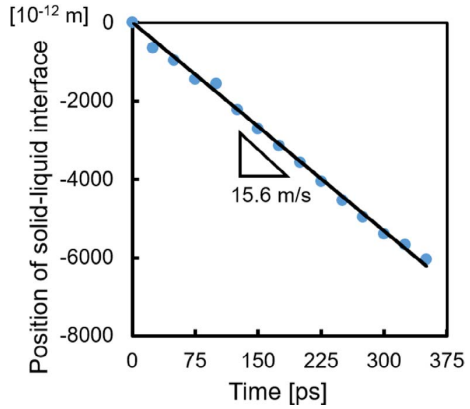

Fig. 2. Position of the solid-liquid interface as a function of time for the solid-liquid biphasic system of pure Al at 910 K. Time and position at the start time of data sampling are set to be zero in the graph. (Online version in color.)

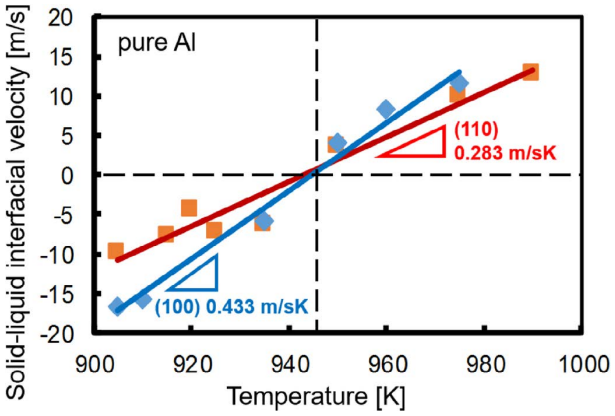

Fig. 3. Solid-liquid interfacial velocity as a function of temperature for (100) (diamonds) and (110) (squares) orientations in the solid-liquid biphasic system of pure Al. Positive values of the interfacial energy represent the melting in the figure. (Online version in color.)

Al system. The kinetic coefficients of the solid-liquid interface of Cu for (100) and (110) orientations are estimated to be 0.193 and 0.131 m/sK, respectively. Again, the kinetic coefficient for the (100) orientation is larger than that of the (110) orientation for the pure Cu system. In the same manner of the pure Al case, the melting point of Cu for this potential is estimated to be 1 441 K, where the experimental value of the melting point of pure Cu is 1 357.77 K. The obtained melting point of Al and Cu from the present atomistic simulations are close to the experimental values, which satisfy the reliability of the present simulation results.

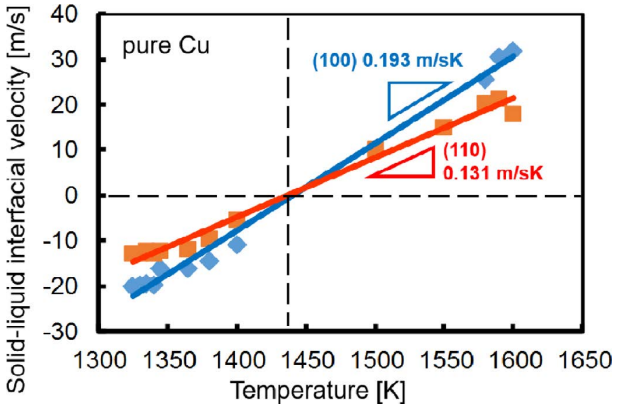

Fig. 4. Solid-liquid interfacial velocity as a function of temperature for (100) (diamonds) and (110) (squares) orientations in the solid-liquid biphasic system of pure Cu. Positive values of the interfacial energy represent the melting in the figure. (Online version in color.)

Table 1 shows melting points and the kinetic coefficients of Al and Cu from this study and representative literatures.[39] Mendelev *et al.*[39] calculated the melting points and the kinetic coefficients of Al and Cu using the interface temperature. They employed the EAM potential varying some parameters in the potential and showed different melting points and kinetic coefficients. The melting point of Al in this study is close to that from Mendelev *et al.*,[39] whereas that of Cu in this study is overestimated to that from the same literature.[39] The first possible reason of this discrepancy is the difference in the definition of the zero velocity temperature between the case using the interface temperature and the thermostat set point temperature. As the second reason, the NVT constant ensemble is employed during the propagation of the solid-liquid interface in the literature,[39] whereas the NPT constant ensemble is employed in this study. It is reported[38,39] that the kinetic coefficient of the solid-liquid interface obtained by using the interface temperature is nearly two times to that using the thermostat set point temperature. Also, it is reported that using the

Table 1. Melting points (T_m) and the kinetic coefficients (KC) of Al and Cu from this study and representative literatures.[8,30,36,38,39,42,57] TST and IT represent the thermostat set temperature and the interface temperature, respectively. The hard sphere (HS) unit is defined as $(k_B/mT_m)^{1/2}$.

Materials	Potentials	Temperature	T_m [K] NVT[39]	T_m [K] NVE[57]	T_m [K] NPT	KC: $\mu(100)$ [m/sK] [HS unit]*	KC: $\mu(110)$ [m/sK] [HS unit]*	Ratio $\frac{\mu(100)}{\mu(110)}$
Al (this work)	EAM[51,58]	TST	–	–	945	0.433	0.283	1.53
Cu (this work)	EAM[51,58]	TST	–	–	1 441	0.193	0.131	1.47
	EA[59]	IT	925	925	–	0.68	0.594	1.15
	MSAHM[58]	IT	940	940	–	1.102	0.937	1.18
Al[39]	Al′[51,60]	IT	534	535	–	1.099	1.259	0.86
	Al″[51,60]	IT	932	932	–	0.231	0.237	0.97
	Al2[51]	IT	930	929	–	1.703	1.424	1.20
Al[36]	SL[61]	TST	–	–	–	0.84*	0.59*	1.42
	ABCHM[51]	IT	1 356	1 356	–	0.75	0.528	1.42
Cu[39]	MMPVK[62]	IT	1 323	1 323	–	0.727	0.582	1.25
	Cu1[51]	IT	1 354	1 353	–	0.627	0.479	1.31
Cu[8]	FBD[46]	TST	–	–	–	0.46	0.27	1.71
Ni[39]	VC[63]	IT	1 624	1 622	–	0.672	0.586	1.15
	FBD[46]	IT	1 707	1 709	–	0.719	0.507	1.42
Ni[38]	FBD[46]	TST	–	–	–	0.36	–	–
	FBD[46]	IT	–	–	–	0.71	–	–
Ni[36]	FBD[46]	TST	–	–	–	1.25*	0.89*	1.41
Au[36]	VC[63]	TST	–	–	–	1.31*	0.8*	1.6
Au[42]	EPT[64]	TST	–	–	–	0.231	0.155	1.49
HS[36]	–	TST	–	–	–	1.44*	1.10*	1.31
Fe[30]	FS[30]	TST	–	–	–	0.325	0.246	1.32

interface temperature approach, the anisotropy of the kinetic coefficient of Al and Cu according to the crystallographic orientations is very small.[38,39] Therefore, we note that the estimation of kinetic coefficient is sensitive to the methodology. Moreover, the analytical expression for the growth velocity of a solid-liquid interface[34] was confirmed by the molecular dynamics simulations for the (100) and (110) orientations, where the expected $\sqrt{2}$ ratio between the kinetic coefficient was well recovered for several metals such as Ni, Ag and Au.[18,42] The value of kinetic coefficient for the hard sphere system calculated using the classical density functional theory along the (100) and (110) orientations are 0.92 and 0.65, respectively and the ratio $\frac{\mu_{100}}{\mu_{110}} = 1.415$.[66] The ratio of kinetic coefficients, $\frac{\mu_{100}}{\mu_{110}}$ of different metals using the thermostat set point temperature, *e.g.*, Ni,[36] Au,[42] Fe,[30] hard sphere,[36] Cu[18] are mostly in the range 1.31–1.71. The anisotropy ratio in this study is also within this range for both Al (1.53) and Cu (1.47) cases.

3.2. Kinetic Coefficient of Al Rich Part of Al–Cu Alloys

Next, the solid-liquid interfacial velocity for solid-liquid biphasic systems of Al-rich Al–Cu alloys is examined. In general, the MD simulation is limited to the phenomena with a timescale of pico- and nano-seconds. Therefore, it is out of range of the MD simulation for the discussion of the solute diffusion in the solid phase. That is, it is not straightforward to obtain the equilibrium solute partition naturally at the solid-liquid interface when two phases contact each other. Therefore, the reproduction of equilibrium partition ratio for the interatomic potential is non-trivial in general. There are some literatures discussing the solute partition at the solid-liquid interfacial energy during the solidification by non-equilibrium MD simulations.[67–69] In these studies, solute segregation happens at the solid-liquid interface only when the interfacial velocity is very small (less than one to five m/s) and solute trapping happens as the interfacial velocity increases. On the other hand, the change in the solid-liquid interfacial velocity with respect to wide range of temperature is required for the estimation of the kinetic coefficient. Therefore, we note that the kinetics of the solid-liquid interface focused on in this study is for the condition of the partitionless solidification and melting.

Figure 5 shows the snapshots of the movement of the solid-liquid interface with the (100) orientation for Al–1.0at%Cu alloy at 915 and 965 K, respectively. It is confirmed from the snapshot that the movement of solid liquid interfacial velocity for Al–1.0at%Cu alloy are moderate compared with the case of pure Al as shown in Fig. 1. The existence of impurity (*i.e.*, Cu) decreases the velocity of the solid-liquid interface even if the amount of impurity is small. **Figure 6** shows the temperature dependence of the solid-liquid interfacial velocity. Error bars in the figure show the standard deviation for four replicate calculations. From these plots, we obtain the slope to be 0.119 m/sK. This slope is called effective kinetic coefficient, which is much smaller than the kinetic coefficient of pure Al. From the

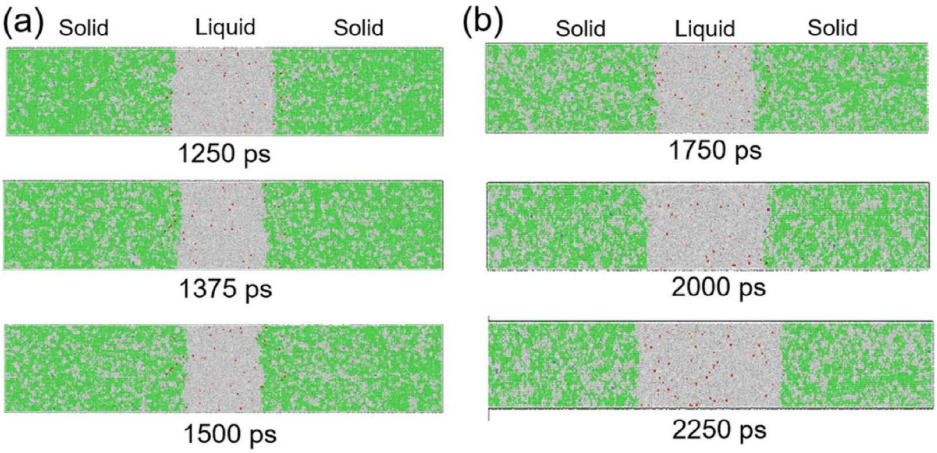

Fig. 5. Snapshots of solid-liquid biphasic system of Al-1.0at%Cu with the (100) plane appearing on the solid-liquid interfaces at (a) 915 K and (b) 965 K, respectively. Green and white atoms represent atoms with fcc and unknown (*i.e.*, liquid) configurations defined as adaptive common neighbor analysis (a-CNA).[55] (Online version in color.)

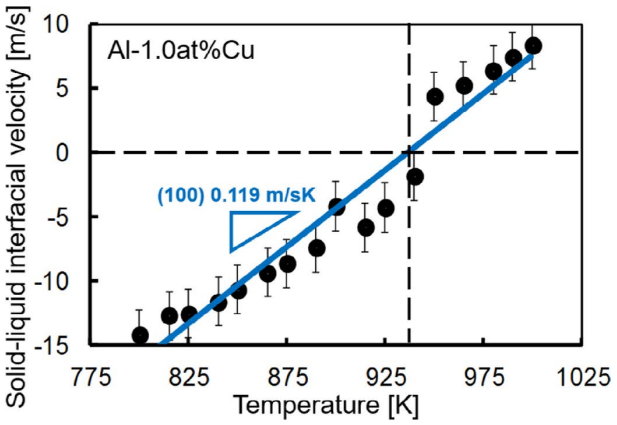

Fig. 6. Solid-liquid interfacial velocity as a function of temperature for the (100) orientation in the solid-liquid biphasic system of pure Al-1.0at%Cu. Error bars represent the standard deviation for four replicate simulations. Positive values of the interfacial energy represent the melting in the figure. (Online version in color.)

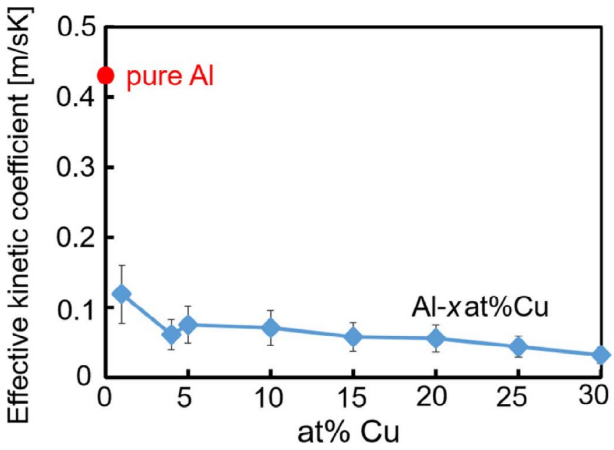

Fig. 7. Effective kinetic coefficient as a function of Cu concentration (at%) for Al–Cu alloys. (blue diamonds). The kinetic coefficient for pure Al is also plotted for comparison (red circle). (Online version in color.)

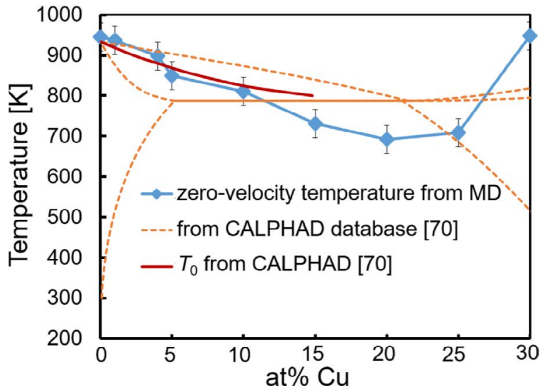

Fig. 8. Zero-velocity temperature at which the solid-liquid interface does not move as a function of Cu concentration (at%). Solidus, liquidus and T_0 lines between fcc and liquid phases from CALPHAD database[70] are shown for comparison. (Online version in color.)

fitted line, the temperature at which the solid-liquid interfacial velocity becomes zero is estimated to be 936 K. It is called zero-velocity temperature in this paper. The physical meaning of the zero-velocity temperature is discussed later. Using the same procedure, the effective kinetic coefficients for Al-rich part of Al–Cu alloys up to 30 at% are estimated. **Figure 7** shows the average values of the effective kinetic coefficient of Al–Cu alloys as a function of Cu concentration with error bars showing standard deviation for four replicate calculations. The kinetic coefficient of pure Al is also plotted for comparison. The effective kinetic coefficient of the Al–Cu alloy decreases drastically compared with the kinetic coefficient of pure Al even when the Cu composition is just 1.0 at%. Then, the effective kinetic coefficient decreases gradually with increasing of Cu concentration.

Figure 8 shows the zero-velocity temperature as a function of Cu concentration up to 30 at%. The zero-velocity temperature decreases with increasing the Cu concentration. In the figure, solidus, liquidus and T_0 lines between fcc and liquid phases calculated from CALPHAD database[70] are shown for comparison. Since the zero-velocity temperatures from the MD simulations are closed to T_0 from the CALPHAD database, it is considered that the zero-velocity temperature from the MD simulation is equivalent to T_0. It means the effective partition of the solute does not occur at the solid liquid interface basically within the time scale of the simulation as described above. However, in Fig. 6, there seems a small gap in the interfacial velocity across the zero-velocity temperature. Since the interfacial velocity

is small at temperatures near the zero-velocity temperature, small amount of partition of the solute may be possible. However, it is difficult to catch the clear evidence of the partition in this simulation, since the number of impurity atoms is too small in this simulation to discuss the partition effect quantitatively. Therefore, we do not go inside further discussion on the partition in this study. The partition of the solute at the solid-liquid interface will be studied in the next step with much larger system.

4. Conclusion

By performing the MD simulation of isothermal holding of solid-liquid biphasic system, the partitionless solidification and melting of Al-rich Al–Cu alloys are investigated. The kinetic coefficients of pure Al and Cu for the (100) orientation are higher than those of the (110) orientation, which signifies the anisotropy of crystal growth and melting during their solidification and liquefaction, respectively. Such the anisotropy is responsible for the formation of dendritic structures during the solidification. Minority Cu element in Al–Cu alloys retards the mobility of the solid-liquid interfacial velocity drastically and the kinetic coefficient decreases with increasing the Cu concentration. The zero-velocity temperatures, at which the interfacial velocity becomes zero, for Al-rich Al–Cu alloys are close to T_0 from the CALPHAD database, which shows that there is almost no partition at the solid-liquid interface within the time scale of the simulation since the solid-liquid interfacial velocity is very fast at temperatures away from the equilibrium temperature. The partition at the solid-liquid interface during the solidification will be investigated using a larger calculation system in a next step.

Acknowledgements

This work was supported by Grant-in-Aid for Scientific Research (B) (16H04490) from Japan Society for the Promotion of Science, and the 23rd ISIJ Research Promotion Grants from the Iron and Steel Institute of Japan. This work was also supported in part by MEXT as a social and scientific priority issue (Creation of new functional devices and high-performance materials to support next-generation industries; CDMSI) to be tackled by using post-K computer.

REFERENCES

1) J. S. Langer: *Rev. Mod. Phys.*, **52** (1980), 1.
2) M. E. Glicksman and R. J. Shaefer: *J. Cryst. Growth*, **1** (1967), 297.
3) G. H. Rodway and J. D. Hunt: *J. Cryst. Growth*, **112** (1991), 554.
4) W. Skoda and M. Van Den Tempel: *J. Cryst. Growth*, **1** (1967), 207.
5) T. Ohashi and W. A. Fisher: *Tetsu-to-Hagané*, **61** (1975), 3077.
6) O. Haida and T. Emi: *Tetsu-to-Hagané*, **63** (1977), 1564.
7) H. Mizukami, K. Hayashi, M. Numata and A. Yamanaka: *Tetsu-to-Hagané*, **97** (2011), 457.
8) W. J. Briels and H. L. Tepper: *Phys. Rev. Lett.*, **79** (1997), 5074.
9) J. Bragard, A. Karma, Y. H. Lee and M. Plapp: *Interface Sci.*, **10** (2002), 121.
10) W. Kurz and D. J. Fisher: Fundamentals of Solidification, 4th Rev. Ed., Trans Tech, Aedermannsdorf, (1998), 13.
11) A. Kerrache, J. Horbach and K. Binder: *Europhys. Lett.*, **81** (2008), 58001.
12) C. A. Becker, M. Asta, J. J. Hoyt and S. M. Foiles: *J. Chem. Phys.*, **124** (2006), 164708.
13) R. Sibug-Aga and B. B. Laird: *J. Chem. Phys.*, **116** (2002), 3410.
14) Y. Shibuta, M. Ohno and T. Takaki: *JOM*, **67** (2015), 1793.
15) M. Asta, F. Spaepen and F. van der Veen: *MRS Bull.*, **29** (2004), 920.
16) J. J. Hoyt, A. Karma, M. Asta and D. Y. Sun: *JOM*, **56** (2004), 49.
17) J. J. Hoyt, B. Sadigh, M. Asta and S. M. Foiles: *Acta Mater.*, **47** (1999), 3181.
18) Y. Shibuta, K. Oguchi and M. Ohno: *Scr. Mater.*, **86** (2014), 20.
19) Y. Shibuta, K. Oguchi, T. Takaki and M. Ohno: *Sci. Rep.*, **5** (2015), 13534.
20) Y. Shibuta, S. Sakane, T. Takaki and M. Ohno: *Acta Mater.*, **105** (2016), 328.
21) Y. Shibuta, S. Sakane, E. Miyoshi, S. Okita, T. Takaki and M. Ohno: *Nat. Commun.*, **8** (2017), 10.
22) J. J. Hoyt, M. Asta and A. Karma: *Phys. Rev. Lett.*, **86** (2001), 5530.
23) E. Asadi, M. A. Zaeem, S. Nouranian and M. I. Baskes: *Acta Mater.*, **86** (2015), 169.
24) H. Zhou, X. Lin, M. Wang and W. Huang: *J. Cryst. Growth*, **366** (2013), 82.
25) R. Hashimoto, Y. Shibuta and T. Suzuki: *ISIJ Int.*, **51** (2011), 1664.
26) J. J. Hoyt and M. Asta: *Phys. Rev. B*, **65** (2002), 214106.
27) S. Angioletti-Ubetti: *J. Phys.: Condens. Matter.*, **23** (2011), 435008.
28) D. Y. Sun, M. Asta and J. J. Hoyt: *Phys. Rev. B*, **69** (2004), 174103.
29) J. Liu, R. L. Davidchack and H. B. Dong: *Comput. Mater. Sci.*, **74** (2013), 92.
30) Y. Watanabe, Y. Shibuta and T. Suzuki: *ISIJ Int.*, **50** (2010), 1158.
31) R. L. Davidchack, J. R. Morris and B. B. Laird: *J. Chem. Phys.*, **125** (2006), 094710.
32) X.-M. Bai and M. Li: *J. Chem. Phys.*, **124** (2006), 124707.
33) J. Q. Broughton, G. H. Gilmer and K. A. Jackson: *Phys. Rev. Lett.*, **49** (1993), 1496.
34) E. Burke, J. Q. Broughton and G. H. Gilmer: *J. Chem. Phys.*, **89** (1988), 1030.
35) J. J. Hoyt, B. Sadigh, M. Asta and S. M. Foiles: *Acta Mater.*, **47** (1999), 3181.
36) M. Amini and B. B. Laird: *Phys. Rev. Lett.*, **97** (2006), 216102.
37) D. Y. Sun, M. Asta and J. J. Hoyt: *Phys. Rev. B*, **69** (2004), 024108.
38) J. Monk, Y. Yang, M. I. Mendelev, M. Asta, J. J. Hoyt and D. Y. Sun: *Model. Simul. Mater. Sci. Eng.*, **18** (2010), 015004.
39) M. I. Mendelev, M. J. Rahman, J. J. Hoyt and M. Asta: *Model. Simul. Mater. Sci. Eng.*, **18** (2010), 074002.
40) Y. F. Gao, Y. Yang, D. Y. Sun, M. Asta and J. J. Hoyt: *J. Cryst. Growth*, **312** (2010), 3238.
41) S. M. Foiles, M. I. Baskes and M. S. Daw: *Phys. Rev. B*, **33** (1986), 7983.
42) F. Celestini and J.-M. Debierre: *Phys. Rev. E*, **65** (2002), 041605.
43) T. Fang, L. Wang and Y. Qi: *Phys. Chem. Liq.*, **52** (2014), 342.
44) S. Tateyama, Y. Shibuta and T. Suzuki: *Scr. Mater.*, **59** (2008), 971.
45) S. Tateyama, Y. Shibuta and T. Suzuki: *ISIJ Int.*, **50** (2010), 1211.
46) S. Tateyama, Y. Shibuta, T. Kumagai and T. Suzuki: *ISIJ Int.*, **51** (2011), 1710.
47) B. Wang and H. M. Urbassek: *Comput. Mater. Sci.*, **81** (2014), 170.
48) X. Ou, J. Sietsma and M. J. Santofimia: *Model. Simul. Mater. Sci. Eng.*, **24** (2016), 055019.
49) C. A. Becker, F. Tavazza, Z. T. Trautt and R. A. Buarque de Macedo: *Curr. Opin. Solid State Mater. Sci.*, **17** (2013), 277, http://www.ctcms.nist.gov/potentials, (accessed 2017-08-16).
50) M. S. Daw and M. I. Baskes: *Phys. Rev. B*, **29** (1984), 6443.
51) M. I. Mendelev, M. J. Kramer, C. A. Becker and M. Asta: *Philos. Mag.*, **88** (2008), 1723.
52) X. Y. Liu, C. L. Liu and L. J. Borucki: *Acta Mater.*, **47** (1999), 3227.
53) S. J. Plimpton: *J. Comput. Phys.*, **117** (1995), 1, http://lammps.sandia.gov, (accessed 2017-08-16).
54) A. Stukowski: *Model. Simul. Mater. Sci. Eng.*, **18** (2010), 015012.
55) A. Stukowski: *Model. Simul. Mater. Sci. Eng.*, **20** (2012), 045021.
56) Y. Shibuta and T. Suzuki: *J. Chem. Phys.*, **129** (2008), 144102.
57) J. R. Morris, C. Z. Wang, K. M. Ho and C. T. Chan: *Phys. Rev. B*, **49** (2010), 3109.
58) M. I. Mendelev, D. J. Srolovitz and G. J. Ackland: *J. Mater. Res.*, **20** (2005), 208.
59) X.-Y. Liu, P. P. Ohotnicky, J. B. Adams, C. L. Rohrer and R. W. Hyland: *Surf. Sci.*, **373** (1997), 357.
60) W.-L. Chan, R. S. Averback, D. G. Cahill and Y. Ashkenazy: *Phys. Rev. Lett.*, **102** (2009), 095701.
61) J. B. Sturgeon and B. B. Laird: *Phys. Rev. B*, **62** (2000), 14720.
62) Y. Mishin, M. J. Mehl, D. A. Papaconstantopoules, A. F. Voter and J. D. Kress: *Phys. Rev. B*, **63** (2001), 224106.
63) A. F. Voter and S. P. Chen: *Mater. Res. Soc. Symp. Proc.*, **82** (1987), 175.
64) F. Ercolessi, M. Parrinello and E. Tossati: *Philos. Mag. A*, **58** (1988), 213.
65) G. J. Ackland, D. J. Bacon, A. F. Calder and T. Harry: *Philos. Mag. A*, **75** (1997), 713.
66) L. V. Mikheev and A. A. Chernov: *J. Cryst. Growth*, **112** (1991), 591.
67) Q. Yu and P. Clancy: *J. Cryst. Growth*, **149** (1995), 45.
68) F. Celestini and J.-M. Debierre: *Phys. Rev. B*, **62** (2000), 14006.
69) Y. Yang, H. Humadi, D. Buta, B. B. Laird, D. Sun, J. J. Hoyt and M. Asta: *Phys. Rev. Lett.*, **107** (2011), 025505.
70) N. Saunders: COST 507 - Thermochemical Database for Light Metal Alloys, Vol. 2, ed. by I. Ansara, *et al.*, Office for Official Publications of the European Communities, Luxembourg, (1998), 28.